Analysis of Pilot-in-the-Loop Oscillations Due to Position and Rate Saturations

F. Amato[*], R. Iervolino[*], M. Pandit[†], S.Scala[‡], L.Verde[‡]

[*]Dipartimento di Informatica e Sistemistica
Università degli Studi di Napoli Federico II
Via Claudio 21, 80125, Napoli, Italy
{framato, rafierv}@unina.it

[†]Control and Signal Processing Group
University of Kaiserslautern
P.O.BOX 30 49, D-67653, Kaiserslautern, Germany
Pandit@e-technik.uni-kl.de

[‡] Flight Systems Department
Italian Aerospace Research Center
Via Maiorise, 81043, Capua, Italy
{l.verde, s.scala}@cira.it

Abstract

In this paper we deal with the analysis of Category II (nonlinear) Pilot in-the-Loop Oscillations (PIO). PIO phenomena are originated by a misadaptation between the pilot and the aircraft that causes *sustained or uncontrollable oscillations*, which especially occur during some tasks where tight closed loop control of the aircraft is required from the pilot. Category II PIO are those oscillations that can strictly be correlated with the activation of rate and position limiter elements in the closed loop pilot-vehicle system. This kind of nonlinearity is unavoidably present in every aircraft, because of physical constraints of elements such as stick/column deflections, actuators position and rate limiters, limiters in the controller software and so on. In this paper we propose an approach, based on the describing function technique, to evaluate the nonlinear effects of the simultaneous presence of position and rate saturations in the control loop. The X-15 landing flare PIO is used as test case to demonstrate the effectiveness of the method.

1. Introduction

The introduction of modern digital fly-by-wire flight control systems has increased the potential for adverse interactions between the human pilot and the aircraft dynamics. These phenomena have been called Pilot-in-the-Loop Oscillations (PIO), and are formally defined in US military standard documents, [1] and [2], as *sustained or uncontrollable oscillations resulting from the efforts of the pilot to control the aircraft.*

To facilitate a clearer understanding of PIO through a systematic study, a classification was recently introduced [3]:

- Category I: Essential linear pilot-vehicle system oscillations.
- Category II: Quasi-linear pilot-vehicle system oscillations with rate and/or position limiting.
- Category III: Essential non-linear pilot-vehicle system oscillations, such as multiple nonlinearities, transitions in pilot behaviour, etc. .

In this paper we focus on Category II PIO analysis, in which it is assumed that PIO are mainly characterised by sustained, quasi-sinusoidal limit cycles due to the presence of rate and amplitude limiting elements [4], [5]. This kind of nonlinearity is unavoidably present in every aircraft, because of physical constraints of elements such as stick/column deflections, actuator position and rate limiters, limiters in the controller software and so on. In particular, actuator rate limiters, that are placed on the control servo commands in order to prevent the hydraulic servos from rate limiting, have been indicated as the significant contributors to various recent high profile PIO incidents/accidents (YF22 [6], Gripen [7]).

Because of the highly destructive potential of the PIO phenomenon, a great effort has been spent in the last years in many research programs, both in USA and Europe [3], [4], [5], [8] to study PIO, in order to derive methods which would be able to predict the tendency of aircraft to develop PIO.

Among all, we can distinguish methods based on Robust Stability Analysis (RSA) [9], [10] and methods based on the Sinusoidal Input Describing Function (SIDF). In this paper we present a SIDF based approach.

Research on limit cycle analysis of nonlinear systems through SIDF has been performed over many years [11], but new studies have been conducted in the last years to better understand the particular problem of PIO caused by rate and amplitude limited actuators [8], [12], [15], [17].

In [8] and [12] a first deep understanding of PIO phenomena in the case of a single nonlinearity in the loop, a pure rate limiting element – i.e. a rate limiting nonlinearity with an infinite bandwith actuator or a software rate limit [13],[14] – is provided. The development of a simple sinusoidal input / triangle output describing function (the *fully rate saturated case* [12]) has lead to the Open Loop Onset Point (OLOP) criterion, the only validated criterion for Category II PIO nowadays.

In [15] a SIDF is defined for the case of finite bandwith closed-loop actuator with only rate limiting [13]; the paper employs exact SIDF calculation to analyse the limit cycle potential of a system that is otherwise linear.

To illustrate the contribution of our paper, let us refer to the usual scheme for the analysis of Category II PIO depicted in Figure 1 [12]. This scheme represents the pilot-vehicle outer loop, with the pilot gain K_P (the pilot *synchronous precognitive behaviour* [12]), the series of the position saturation followed by the rate saturation of pilot control commands, in the following indicated as PRS (Position Rate Saturation), and the aircraft dynamics block $G_S(s)$ (including the flight control system).

The first contribution of this paper consists of considering the effects of the simultaneous presence in the loop of two

nonlinearities: amplitude saturation and rate limiter of the pilot commands. PIO analysis in the presence of multiple nonlinearities has been performed in [17] by assuming the nonlinearities are independent each other; this can obviously introduce a strong optimism in the analysis result. We propose a novel method, which allows one to take into consideration the interactions between the nonlinear elements. Such a method considers the PRS block as a unique nonlinear dynamic element, whose exact SIDF is computed by performing an analytical derivation following the guidelines of [16]. This approach also renders the limit cycle detection extremely efficient from a numerical point of view.

An application to the X-15 landing flare PIO [18] illustrates the effectiveness of the proposed method. Finally, how the method can be used in the design stage, to give requirements on the actuators characteristics in order to avoid Category II PIO proneness, is also shown.

2. Describing Function Analysis: The Position-Rate Saturation Case

Let us consider the PRS system in Figure 1, and denote by R_L the value of the rate limit and by P_L the value of the input amplitude saturation. It is possible to compute the SIDF of the series of the two nonlinear elements in Figure 1 by considering the two blocks as a unique nonlinear system. We shall show in Section 3 that this approach leads to very good results in terms of limit cycle detection.

For the PRS system, the analytical expression of the SIDF has been derived, as described below.

2.1 Analytical derivation of the PRS describing function

The SIDF of a PRS block depends on the actual values of position and rate limits, and, since the PRS system is a dynamic nonlinearity, also on both input amplitude and frequency.

Let us consider the output of the PRS block to a sinusoidal input $x(t) = X\sin(\omega t)$ of given amplitude X and frequency ω.

The steady state component of this output, say $u(t)$, is a periodic signal of the same period of the input $x(t)$. The SIDF of the PRS is the ratio of the fundamental harmonic of the periodic output signal $u(t)$ (in phasor form) to that of the input sinusoidal signal $x(t)$; it can be obtained in symbolic form from sine and cosine Fourier integrals

$$F(X,\omega) = \frac{Re\,F}{X} + j\frac{Im\,F}{X}$$

$$Re\,F = \frac{2}{\pi}\int_0^{\pi} u\left(\frac{\theta}{\omega}\right)\cdot \sin\theta\; d\theta$$

$$Im\,F = \frac{2}{\pi}\int_0^{\pi} u\left(\frac{\theta}{\omega}\right)\cdot \cos\theta\; d\theta$$

where $\theta = \omega t$.

The introduction of the following change of variables facilitates the analytical derivation of the SIDF [16]

$$\beta = \frac{R_L}{X\omega};\ \rho = \frac{P_L}{X} \rightarrow F(X,\omega) = n(\beta,\rho)\big|_{\beta=\frac{R_L}{X\omega};\rho=\frac{P_L}{X}} \qquad (1)$$

Indeed the computation of the Fourier integrals is simplified if one separates the possible output shapes according to the different range of values of β and ρ:

a) **CASE $\beta \geq 1$ and $\rho \geq 1$**: the position and rate saturations never activate.
b) **CASE $\beta \geq 1$ and $\rho < 1$**: the input signal is only limited in amplitude and the SIDF depends only on ρ.
c) **CASE $\beta < 1$ and $\rho \geq 1$**: the input signal is only rate limited and the SIDF depends only on β.
d) **CASE $\beta < 1$ and $\rho < 1$**: the input signal is both amplitude and rate limited and the SIDF depends both on β and ρ.

Let us detail the analytical derivation of the SIDF for each of the above mentioned four cases.

(a) **CASE $\beta \geq 1$ and $\rho \geq 1$**

In this case the sinusoidal input $x(t)$ is neither amplitude nor rate limited, i.e. $u(t) = x(t)$. Hence

$$n(\beta,\rho) = 1.$$

(b) **CASE $\beta \geq 1$ and $\rho < 1$**

In this case the sinusoidal input $x(t)$ is only amplitude limited, i.e. the PRS block reduces to a simple position saturation block, for which

$$n(\beta,\rho) = \frac{2}{\pi}\left[\sin^{-1}\rho + \rho\,\cos\left(\sin^{-1}\rho\right)\right].$$

(c) **CASE $\beta < 1$ and $\rho \geq 1$**

In this case only the limitation of the derivative of the sinusoidal input $x(t)$ is effective. We can distinguish two output shapes [16] (see Figure 2). There exists a critical value of β, say β_{crit},

$$\beta_{crit} = \frac{1}{\sqrt{1+\frac{\pi^2}{4}}} \cong 0.537$$

which discriminates the two possible output behaviours, the one for $\beta < \beta_{crit}$ and the one for $\beta \geq \beta_{crit}$ [16], and therefore the two different expressions of the SIDF.

When $\beta \geq \beta_{crit}$, we have (see Figure 2)

$$\theta = \omega t,\quad \theta_0 = \omega t_0,\quad \theta_1 = \omega t_1,\quad \omega = \frac{2\pi}{T}$$

$$u\left(\frac{\theta}{\omega}\right) = \begin{cases} X\sin\theta, & \theta_1 \leq \theta < \theta_0 + \pi \\ X\sin\theta_0 + \dfrac{R_L}{\omega}(\theta - \theta_0), & \theta_0 \leq \theta < \theta_1 \end{cases}$$

where θ_0 and θ_1 are the solutions of the equations:

$$\dot{u}(t_0) = R_L = \dot{x}(t_0) = X\omega\cos\theta_0$$

and

$$u(t_1) = X\ sin\theta_0 + \frac{R_L}{\omega}(\theta_1 - \theta_0) = x(t_1) = X\ sin\theta_1$$

relative to the interval $[t_0\ ,\ t_1]$ where the rate limit is active. Therefore

$$n(\beta,\rho) = \frac{2}{\pi}\{(sin\theta_0 - \beta\theta_0)(cos\theta_0 - cos\theta_1) + \beta(sin\theta_1 - \theta_1\ cos\theta_1 - sin\theta_0 + \theta_0\ cos\theta_0) + \frac{1}{2}(\theta_0 + \pi - sin\theta_0\ cos\theta_0 - \theta_1 + sin\theta_1\ cos\theta_1)\} + j\frac{2}{\pi}\{(sin\theta_0 - \beta\theta_0)(sin\theta_1 - sin\theta_0) + \beta(\theta_1 sin\theta_1 + cos\theta_1 - \theta_0 sin\theta_0 - cos\theta_0) + \frac{1}{2}(sin^2\theta_0 - sin^2\theta_1)\}$$

When $0<\beta < \beta_{crit}$ we have, according to the situation depicted in Figure 2, that the output keeps the saw tooth form (the *fully rate saturated case* [12])

$$u\left(\frac{\theta}{\omega}\right) = Xsin\theta_0 + \frac{R_L}{\omega}(\theta - \theta_0) \quad \theta_0 \le \theta < \theta_0 + \pi\ ,$$

where θ_0 is determined by

$$Xsin(\theta_0 + \pi) = Xsin\theta_0 + \frac{R_L}{\omega}\pi\ .$$

Hence

$$n(\beta,\rho) = 2\beta^2 - j\frac{4}{\pi}\beta\sqrt{1 - \frac{\beta^2\pi^2}{4}}\ .$$

(d) **CASE $\beta < 1$ and $\rho < 1$**

If the input signal $x(t)$ is rate and amplitude limited, then the output signal oscillations $u(t)$ has the behaviour shown in Figure 3 and Figure 4.

One can distinguish two different families of output forms by looking at the current value of ρ; indeed, there exists one critical value of ρ

$$\rho_{crit} = \frac{\frac{\pi}{2}}{\sqrt{1 + \frac{\pi^2}{4}}} \cong 0.844\ ,$$

such that if $0<\rho \le \rho_{crit}$ the situation is one depicted in Figure 3, while if $\rho_{crit} \le \rho < 1$ the situation is one of those depicted in Figure 4.

In particular, when $0 < \rho \le \rho_{crit}$, we have four sub-cases depending on which of the following intervals the current value of β belongs

1. $\beta_{crit}(\rho) \le \beta < 1$;
2. $\sqrt{1-\rho^2} \le \beta < \beta_{crit}(\rho)$;
3. $\frac{2\rho}{\pi} \le \beta < \sqrt{1-\rho^2}$;
4. $0 < \beta < \frac{2\rho}{\pi}$,

where we define $\beta_{crit}(\rho)$ as the value of β which satisfies the following condition

$$-sin(cos^{-1}\beta) + \beta\ cos^{-1}\beta + \beta\ sin^{-1}\rho = \rho\ .$$

Conversely, when $\rho_{crit} \le \rho < 1$, we have four sub-cases depending on which of the following intervals the current value of β belongs

1. $\beta_{crit}(\rho) \le \beta < 1$;
2. $\beta^*(\rho) \le \beta < \beta_{crit}(\rho)$;
3. $\tilde{\beta} \le \beta < \beta^*(\rho)$;
4. $0 < \beta < \tilde{\beta}$

where we define $\beta^*(\rho)$ the value of β which satisfies the following condition

$$-sin(cos^{-1}\beta) + \beta\ cos^{-1}\beta - \beta\ sin^{-1}\rho + \beta\pi = \rho$$

and $\tilde{\beta}$ is

$$\tilde{\beta} = \frac{1}{\sqrt{1 + \frac{\pi^2}{4}}} \cong 0.537\ .$$

The analytical expression of $n(\beta,\rho)$ is determined following the same procedure of Case (c) above.

3. Limit Cycle Analysis: The X-15 Test Case

The SIDF technique has been applied to the problem of limit cycling detection for the X-15 PIO which occurred during a landing flare [18]. The model of the aircraft with a pure rate limiter and a stick deflection limit is shown in Figure 1. The numerical values of the elements in the block diagram are:

$$G_S(s) = \frac{3.476(s + 0.0292)(s + 0.883)}{(s^2 + 0.019s + 0.01)(s^2 + 0.8418s + 5.29)}$$
$$R_L = 15\ deg/\ sec \qquad (2)$$
$$P_L = 30\ deg$$

Referring to the pilot-vehicle systems in Figure 1, the following set of equations defines the condition of a sinusoidal limit cycle at the input of the pilot gain block:

$$K_P F(X,\omega)\, G(j\omega) = -1\ , \qquad (3)$$

where K_P is the pilot gain, $F(X,\omega)$ is the SIDF of the PRS element, and $G_S(j\omega)$ is the transfer function of the remaining linear part of the open-loop system. It is assumed that in the real situation to be analysed the pilot gain is uncertain, but time-invariant, i.e. the pilot holds its

gain fixed to some particular value during the critical manoeuvre, the actual value depending on the flight phase and the particular pilot himself. This follows the synchronous precognitive behaviour assumption for the pilot model. It is further assumed, that, although the actual pilot gain is uncertain, the range in which it can take values is known. The assumed range, similar to what is done in the OLOP criterion [12], is computed from the linear aircraft response as the range of pilot gains for which the phase margin of the loop transfer function is in the interval from 70° (lower pilot gain) to 20° (higher pilot gain). It is indeed assumed that the pilot would try to control the aircraft with such a range of gains, because different values would lead to problems already within the linear regime, such as for instance Category I PIO.

The harmonic balance equation (3) has been solved for several values of K_P to find the parameters, X^* and ω^*, of the limit cycle. Then, time simulations of the nonlinear model of Figure 1 have been run for the given values of K_P, to make a comparison between the actual (simulated) limit cycle amplitude and frequency and the ones estimated via SIDF analysis.

The results for the X-15 aircraft are shown in the two plots of Figure 5. The two plots presented show respectively: (a) the pilot gain K_P versus the frequency of the limit cycle ω_{lc}; (b) the pilot gain K_P versus the amplitude of the limit cycle. The diamonds correspond to the SIDF analysis results and the circles to the time-simulations results. Two solid horizontal lines in the first and third plots have been drawn in correspondence of the pilot gains for which the phase margin of the linear aircraft model is, starting from the bottom, 70° or 20°. It is important to note that when performing a PIO analysis, one should assess both Category I and Category II PIO tendencies. For pilot gains above the one for the lower phase margin, the gain margin of the linearised aircraft is so poor that the aircraft will be certainly subject to Category I PIO. This fact suggests to disregard, in the Category II PIO analysis, the pilot gains above this value.

There is a good adherence between SIDF analysis predictions and time-simulations, due to the sufficiently low pass filter characteristics of the linear part of the closed loop systems.

The pilot gain vs. frequency plot shows that limit cycles can be generated in the system with *medium-high* pilot gains, i.e. with pilot gains in the upper part of the range between the low and high pilot gains. The frequency corresponding to the limit cycle arising at the lower pilot gain is about 2.7 rad/s, well within the frequency range of activity of a standard pilot. This result is important to note, since in this analysis we have used a pure gain pilot model, i.e. with no cut-off frequency.

It should also be noted that, for each pilot gain above the minimum value for which limit cycles are predicted, two limit cycles exist. The limit cycle of lower frequency is of higher amplitude. This oscillation is a stable limit cycle, as time simulations confirm. The other limit cycle, of higher frequency and lower amplitude is unstable, and it cannot be revealed by time simulations. To further show this point, several phase plane plots are included, for various values of the pilot gain.

Figure 6 presents the case with pilot gain K_P = 2 and large initial conditions (large initial attitude error), Figure 7, Figure 8, and Figure 9 present the case with pilot gain = 3 and large, medium and small initial conditions respectively. It can be noted that large and medium initial conditions lead to the same stable limit cycle, while the small initial condition converges to the origin. This situation confirms that an unstable limit cycle exist between the medium and small initial conditions trajectories. Figure 10, Figure 11, and Figure 12 present similar results with pilot gain = 6. This value is higher than the maximum pilot gain used for the PIO analysis, and it is presented here to highlight that, when the pilot gain increases, the region of initial conditions from which the stable limit cycle is reached comprises points of smaller and smaller amplitude. Indeed the unstable limit cycle, and the region of asymptotic stability around the origin included in it, shrink while the pilot gain is increased, as estimated from Figure 5.

Note also that the limit cycle amplitude shown in the plots is quite high, in particular for the pilot gain in the above indicated range, showing that these limit cycles are potentially disastrous. In summary the SIDF analysis performed here predicts that the investigated X-15 configuration have Category II PIO tendency, which confirms the flight results presented in [19].

Finally we highlight that the method can also be used during the design stage, in order to obtain an estimate of the lowest maximum rate to require from the actuators.

Figure 13 presents, in the plane of pilot gain versus limit cycle frequency, the result of the SIDF analysis of the X-15 repeated for two values of the rate limit. The first value, R_L =15°/s, is the value of the previous analysis, for which PIO proneness was predicted. The analysis has been repeated to find the value of rate limit for which the curve of the limit cycle parameters in the (ω_{lc} , K_P) plane is completely above the horizontal line of the maximum pilot gain, corresponding to 20° of phase margin of the linearised model. The second curve is obtained for rate limit R_L =85°/s . It can be predicted that, if this value of the rate limit is selected, the aircraft should be free from Category II PIO.

The time simulations of Figure 14 confirm this prediction. They are obtained for the previous two values (15°/s and 85°/s) of the rate limit and with the maximum pilot gain of the PIO analysis (K_P = 3.5), corresponding to 20° of phase margin of the linearised model. The predicted benefit of raising the rate limit is confirmed.

4. Conclusions

A SIDF approach for the analysis of Category II PIO with the simultaneous presence of rate and position limiting of the pilot commands has been presented. The novelty, with respect to previous papers, is the development of a technique to directly obtain the expression of the SIDF of the PRS system. The effectiveness of the proposed method is illustrated by the X-15 PIO case study; indeed a very

good agreement was reached between the limit cycle frequency and amplitude predicted by the analysis and that experienced in flight. Moreover, an example of the application of the method to actuator design has been presented.

5. References

[1] Military Specification (1980), *Flying Qualities of Piloted Airplanes*, MIL-F-8785 C, Wright Patterson AFB.

[2] Military Specification (1990), *Flying Qualities of Piloted Aircraft*, MIL-STD-1797 A, Wright Patterson AFB.

[3] D. McRuer et al., *Aviation Safety and Pilot Control. Understanding and Preventing Unfavorable Pilot-Vehicle Interactions*, ASEB National Research Council, National Academy Press, Washington D.C., 1997.

[4] M.R. Anderson and A.B. Page, "Unified Pilot-Induced Oscillation Theory, Volume III: PIO Analysis using Multivariable Methods," *WL-TR-96-3030*, Wright Laboratory, Wright-Paterson Air Force Base, Ohio, 1995.

[5] D.H. Klyde, D.T. McRuer and T.T. Myers, "Unified Pilot-Induced Oscillation Theory, Volume I: PIO Analysis with Linear and Nonlinear Effective Vehicle Characteristics, including Rate Limiting," WL-TR-96-3028, Wright Laboratory, Wright-Paterson Air Force Base, Ohio, 1995.

[6] M.A. Dornheim, "Report Pinpoints Factors Leading to YF-22 Crash," *Aviation Week Space Technology*, pp. 53-54, Nov. 9, 1992.

[7] J.M. Lenorovitz, "Gripen Control Problems Resolved through In-Flight, Ground Simulations," *Aviation Week Space Technology*, pp. 74-75, June 18, 1990.

[8] H. Duda, "Minutes on a Workshop on Pilot-in-the-Loop Oscillations held at DLR, Braunschweig on June 12-13th, 1997," *DLR IB 111-97/25*, Braunschweig, 1997.

[9] F. Amato, R. Iervolino, S. Scala and L. Verde, "A Robust Stability Analysis Approach for Prediction of Pilot In The Loop Oscillations," in *Proc. 1999 European Control Conference*, Karlsruhe, Germany, Sept. 1999.

[10] F. Amato, R. Iervolino, S. Scala and L. Verde, "New criteria for the analysis of PIO based on Robust Stability methods," in *Proc. 1999 AIAA Guidance Navigation and Control Conference*, Portland (OR), Aug. 1999.

[11] D.P. Atherton, *Nonlinear Control Engineering*, Van Nostrand Reinhold Co., London & New York, 1975.

[12] H. Duda,"Prediction of Pilot-in-the-Loop Oscillations Due to Rate Saturation," *Journal of Guidance, Control, and Dynamics*, vol. 20, no. 3, May-June 1997.

[13] J.M. Berg, K.D. Hammett, C.A. Schwartz and S.S. Banda, "An Analysis of the Destabilizing Effect of Daisy Chained Rate-Limited Actuators," *IEEE Transaction on Control System Technology*, vol. 4, no. 2, Mar. 1996.

[14] L. Rundqwist and K.S.-Gunnarsson, "Phase Compensation of Rate Limiters in Unstable Aircraft," in *Proc. of the 1996 IEEE International Conference on Control Applications*, Dearborn, MI, Sept. 15-18, 1996.

[15] D.H. Klyde, D.T. McRuer, and T.T. Myers, "Pilot-Induced Oscillation Analysis and Prediction with Actuator Rate Limiting," *Journal of Guidance, Control, and Dynamics*, vol. 20, no. 1, Jan.-Feb. 1997.

[16] M. Pandit, "Stability of Control Systems Employing Bang-Bang Actuators with Integral Feedback," (in German) *Automatisierungstechik* , vol. 35, no. 7, 1987.

[17] M.R. Anderson, "Pilot-Induced Oscillations Involving Multiple Nonlinearities," *Journal of Guidance, Control, and Dynamics*, vol. 21, no. 5, Sept.-Oct. 1998.

[18] G.J. Matranga, "Analysis of X-15 Landing Approach and Flare Characteristics Determined from the first 30 Flights," *NASA TN D-1057*, Washington, 1961.

[19] I.L. Ashkenas, H.R. Jex and D.T. McRuer, "Pilot-Induced Oscillations: Their Cause and Analysis," *NORAIR Rept. NOR-64-143* (also *Systems Technology, TR-239-2*), June 1964.

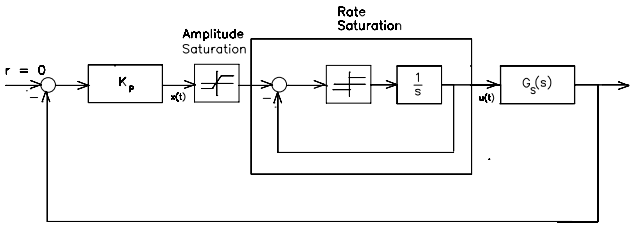

Figure 1: PIO scheme for PIO analysis.

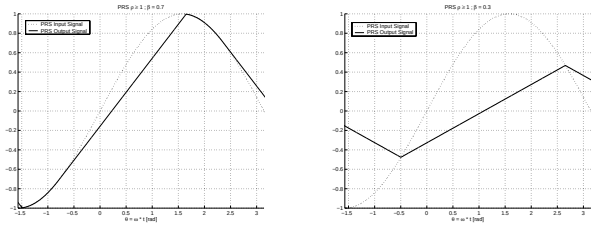

$\beta_{crit} \le \beta < 1$ $\qquad$ $0 < \beta < \beta_{crit}$

Figure 2: PRS output shapes for $\rho \ge 1$ and $\beta < 1$

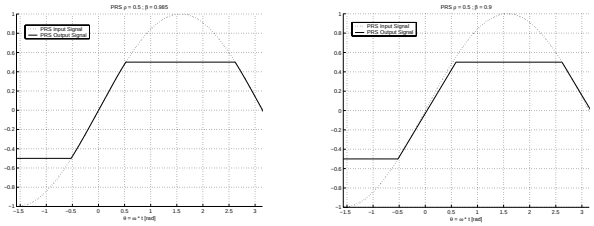

$\beta_{crit}(\rho) \le \beta < 1$ $\qquad \sqrt{1-\rho^2} \le \beta < \beta_{crit}(\rho)$

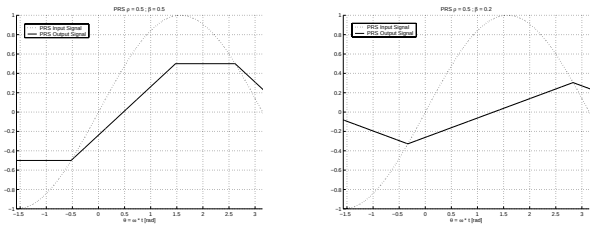

$\frac{2\rho}{\pi} \le \beta < \sqrt{1-\rho^2}$ $\qquad 0 < \beta < \frac{2\rho}{\pi}$

Figure 3. PRS output shapes for $\rho < 1$ and $\beta < 1$ (case $\rho \le \rho_{crit}$)

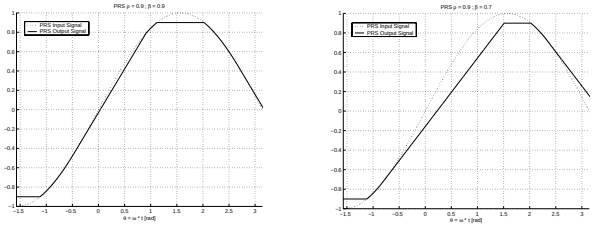

$\beta_{crit}(\rho) \le \beta < 1$ $\qquad \beta^*(\rho) \le \beta < \beta_{crit}(\rho)$

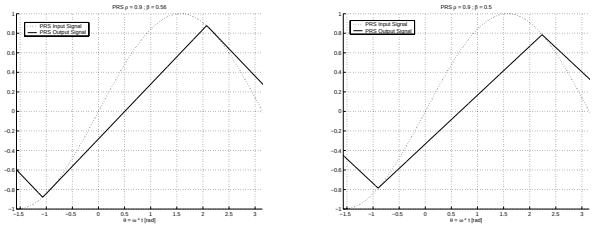

$\tilde{\beta} \le \beta < \beta^*(\rho)$ $\qquad 0 < \beta < \tilde{\beta}$

Figure 4. PRS output shapes for $\rho < 1$ and $\beta < 1$ (case $\rho > \rho_{crit}$)

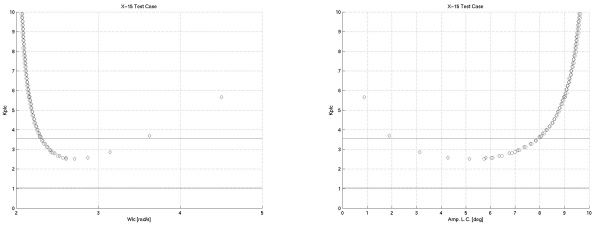

(a) (b)

Figure 5: (a) X-15 pilot gain vs. limit cycle frequency. ; (b) X-15 pilot gain vs. limit cycle amplitude.

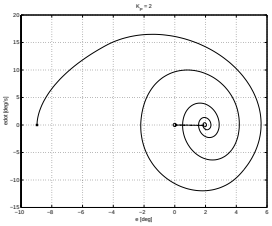

Figure 6: Phase plane plot for pilot gain = 2 and large initial condition

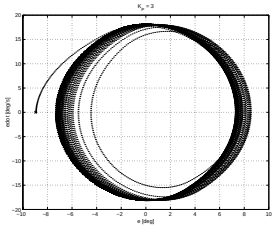

Figure 7:Phase plane plot for pilot gain = 3 and large initial condition

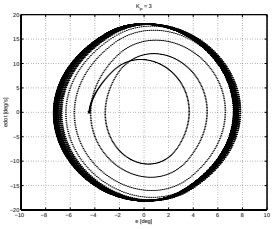

Figure 8: Phase plane plot for pilot gain = 3 and medium initial condition.

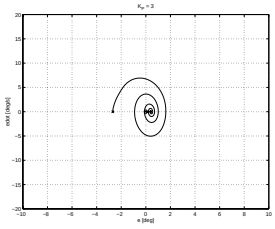

Figure 9: Phase plane plot for pilot gain = 3 and small initial condition

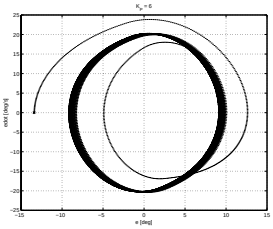

Figure 10: Phase plane plot for pilot gain = 6 and large initial condition.

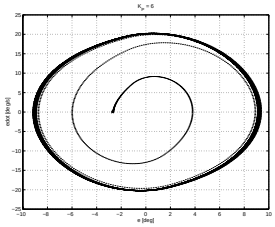

Figure 11: Phase plane plot for pilot gain = 6 and medium initial condition

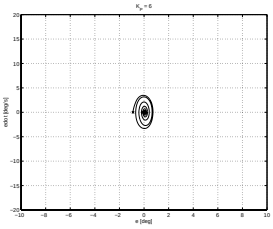

Figure 12: Phase plane plot for pilot gain = 6 and small initial condition

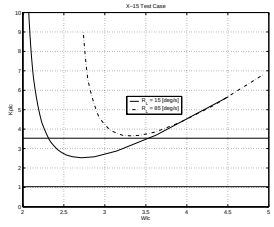

Figure 13: X-15 pilot gain vs. limit cycle frequency for two values of the rate limit

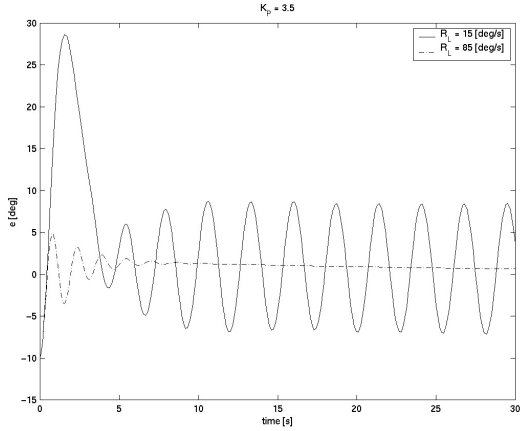

Figure 14: Time simulations of the X-15 for two values of the rate limit.